



HAL
open science

The *Ralstonia solanacearum* type-III effector RipAY targets plant redox regulators to suppress immune responses

Yuying Sang, Yaru Wang, Hong Ni, Anne-Claire Cazalé, Yi-Min She, Nemo Peeters, Alberto P. Macho

► To cite this version:

Yuying Sang, Yaru Wang, Hong Ni, Anne-Claire Cazalé, Yi-Min She, et al.. The *Ralstonia solanacearum* type-III effector RipAY targets plant redox regulators to suppress immune responses. *Molecular Plant Pathology*, 2018, 19 (1), pp.129-142. 10.1111/mpp.12504 . hal-02626870

HAL Id: hal-02626870

<https://hal.inrae.fr/hal-02626870>

Submitted on 22 Jul 2022

HAL is a multi-disciplinary open access archive for the deposit and dissemination of scientific research documents, whether they are published or not. The documents may come from teaching and research institutions in France or abroad, or from public or private research centers.

L'archive ouverte pluridisciplinaire **HAL**, est destinée au dépôt et à la diffusion de documents scientifiques de niveau recherche, publiés ou non, émanant des établissements d'enseignement et de recherche français ou étrangers, des laboratoires publics ou privés.



Distributed under a Creative Commons Attribution 4.0 International License

The *Ralstonia solanacearum* type-III effector RipAY targets plant redox regulators to suppress immune responses

Yuying Sang^{1,2}, Yaru Wang^{1,2}, Hong Ni¹, Anne-Claire Cazalé³, Yi-Min She¹, Nemo Peeters³, and Alberto P. Macho^{1,2*}

¹Shanghai Center for Plant Stress Biology, Shanghai Institutes of Biological Sciences, Chinese Academy of Sciences, Shanghai, China.

²CAS Center for Excellence in Molecular Plant Sciences; Shanghai Institutes of Biological Sciences, Chinese Academy of Sciences, Shanghai, China.

³LIPM, Université de Toulouse, INRA, CNRS, Castanet-Tolosan, France.

* For correspondence: alberto.macho@sibs.ac.cn

(+86) 21-5707818

Running title: RipAY targets redox regulators to suppress immunity

Keywords: *Ralstonia*; type-III effector; redox; plant immunity; glutathione; thioredoxin

Word count (Summary, Introduction, Results, Discussion, Experimental Procedures, Acknowledgements, Table and Figure Legends): 7209

This article has been accepted for publication and undergone full peer review but has not been through the copyediting, typesetting, pagination and proofreading process which may lead to differences between this version and the Version of Record. Please cite this article as an 'Accepted Article', doi: 10.1111/mpp.12504

SUMMARY

The subversion of plant cellular functions is essential for bacterial pathogens to proliferate in host plants and cause disease. Most bacterial plant pathogens employ a type-III secretion system to inject type-III effector (T3E) proteins inside plant cells, where they contribute to the pathogen-induced alteration of plant physiology. In this work, we found that the *Ralstonia solanacearum* T3E RipAY suppresses plant immune responses triggered by bacterial elicitors and by the phytohormone salicylic acid. Further biochemical analysis indicated that RipAY associates *in planta* with thioredoxins from *Nicotiana benthamiana* and Arabidopsis. Interestingly, RipAY displays gamma-glutamyl cyclotransferase (GGCT) activity to degrade glutathione in plant cells, which is required for the reported suppression of immune responses. Given the importance of thioredoxins and glutathione as major redox regulators in eukaryotic cells, RipAY activity may constitute a novel and powerful virulence strategy employed by *R. solanacearum* to suppress immune responses and potentially alter general redox signalling in host cells.

INTRODUCTION

To infect a plant, pathogens need to manipulate host cells to turn an otherwise hostile environment into a niche suitable for pathogen proliferation. For gram-negative bacterial pathogens of plants and animals, an essential means to achieve host manipulation is the type-III secretion system (T3SS), a molecular syringe that injects proteins, termed type-III effectors (T3Es), directly inside host cells (Galan *et al.*, 2014).

Plants have developed a complex immune system capable of perceiving multiple kinds of microbial molecules, which are interpreted as invasion patterns (IPs; Cook *et al.*, 2015). Some bacterial proteins can be perceived directly at the plant cell surface by receptors localized at the plasma membrane, termed pattern-recognition receptors (PRRs; Zipfel, 2014). Bacterial proteins delivered inside plant cells can also be perceived, in a direct or indirect manner, by intracellular receptors containing nucleotide-binding and leucine-rich repeat domains (NLRs; Khan *et al.*, 2016). The activation of these IP receptors leads to an extensive reprogramming of host cells in order to strengthen defences and initiate immune responses (Bigeard *et al.*, 2015, Boller & Felix, 2009, Tsuda & Katagiri, 2010). This immune activation is expected to prevent the proliferation of the perceived bacteria, and prepare plant cells for an efficient defence response against further invading bacteria. To neutralize this plant surveillance system and the subsequent immune responses, successful bacterial pathogens have evolved T3Es that are able to suppress plant immune signalling at multiple levels (Deslandes & Rivas, 2012, Macho & Zipfel, 2015). This immune suppression is supported by the subversion of additional plant functions (Macho, 2016). T3E manipulation of plant cellular functions is key to allow bacterial proliferation and, ultimately, development of disease, but presents the additional risk of T3E perception by NLRs (Khan *et al.*, 2016). The definition of opposite forces that determine the outcome of a plant-bacteria interaction (bacterial virulence activities *versus* plant immune responses) has led to the proposition of a model presenting a complex evolutionary arms race between effectors and plant defence responses (Jones & Dangl, 2006, Win *et al.*, 2012). The complex outcome of this interaction will influence the perception and response to further bacteria at the site of infection and distal tissues.

Plants rely on a balanced cellular environment to maintain basal levels of immune regulators and to mount defence responses after pathogen perception. Redox

regulators efficiently buffer the redox status of plant cells, and play important roles in the activation of immune responses after pathogen perception (Spoel & Loake, 2011). However, our knowledge on whether and how pathogens manipulate redox regulation to cause disease is still scarce.

Ralstonia solanacearum is often considered one of the most destructive bacterial pathogens, causing bacterial wilt disease in more than 250 plant species worldwide (Mansfield *et al.*, 2012). *R. solanacearum* can live for long periods in water or soil, and is able to penetrate plants through the roots. After plant invasion, *R. solanacearum* reaches the vascular system and uses the xylem vessels to colonize the whole plant. Massive bacterial replication and production of exopolysaccharide eventually leads to the collapse of the vascular system, therefore causing severe wilting and plant death (Peeters *et al.*, 2013b). It has been shown that *R. solanacearum* is able to express genes related to the T3SS throughout different stages of the infection process (Monteiro *et al.*, 2012). Interestingly, the versatile lifestyle of *R. solanacearum* and the colonization of different plant organs correlates with a larger number of T3Es compared to other bacterial pathogens: bacteria from a single *R. solanacearum* strain can inject up to 70 T3Es (termed Rips for *Ralstonia* injected proteins) inside plant cells (Peeters *et al.*, 2013a). Although the role of several of these effectors has been studied (Deslandes & Genin, 2014), the relevance and function of most of them remains unknown, and therefore the *R. solanacearum* T3E repertoire constitutes a powerful tool to identify novel bacterial virulence activities and decipher pathogen manipulation of plant functions. One of these T3Es, RipAY, was shown to contribute to *R. solanacearum* virulence in eggplant leaves (Macho *et al.*, 2010). Interestingly, RipAY is widely conserved along the *R. solanacearum* strains sequenced to date (Clarke *et al.*, 2015, Peeters *et al.*, 2013a), and is one of the few Rips that does not trigger hypersensitive response (HR)-like responses in any of the plant genotypes tested (Clarke *et al.*, 2015).

In this work, we studied the potential basis of the virulence activity of RipAY, and found that RipAY suppresses immune responses triggered by bacterial elicitors and the defence-related phytohormone salicylic acid (SA). Further biochemical analysis indicated that RipAY associates with several redox regulators and that the manipulation of plant redox regulation is essential for the observed suppression of immune responses.

RESULTS

RipAY can suppress immune responses

Several T3Es from different bacterial pathogens contribute to the suppression of plant defence responses (Deslandes & Rivas, 2012, Macho & Zipfel, 2015). The activation of plant PRRs by microbial elicitors leads to a plethora of signalling events and immune responses, including an early burst of reactive oxygen species (ROS), and the activation of a cascade of mitogen-activated protein kinases (MAPKs) (Boller & Felix, 2009, Macho & Zipfel, 2014). The peptide flg22 (representative of one of the elicitor domains of bacterial flagellin) is perceived in most plants by a PRR complex formed by the leucine-rich repeat receptor kinases FLS2 and BAK1 (Gómez-Gómez & Boller, 2000, Sun *et al.*, 2013), and is commonly employed to elicit and probe PRR-dependent responses in laboratory conditions. To determine whether RipAY has the potential to suppress elicitor-induced responses in plant cells, we used an *Agrobacterium tumefaciens*-mediated transient expression system in *Nicotiana benthamiana* leaf tissues. Two days after infiltration with *A. tumefaciens*, we observed a strong reduction in flg22-triggered ROS burst in half-leaves expressing RipAY, fused to a green-fluorescent protein (GFP) tag or a hemagglutinin-StreptII (HA-StreptII) tag (Figure 1a, 1b and S1). As controls, we used *A. tumefaciens* carrying constructs to trigger the expression of GFP or GFP-HA-StreptII, infiltrated in the other half of the leaf, allowing a direct comparison with RipAY-expressing tissues (Figure 1a, 1b and S1). Interestingly, RipAY expression did not cause a clear and reproducible suppression of flg22-triggered MAPK activation (Figure S2). This may indicate that RipAY differentially affects responses to flg22, although an influence of the differential sensitivity of the assays to determine the ROS burst and the activation of MAPKs cannot be excluded.

SA plays a major role in the activation of immune responses after the perception of different types of invasion patterns (Vlot *et al.*, 2009). To determine whether RipAY interferes with SA-dependent responses, we measured the expression of the *N. benthamiana* ortholog of the Arabidopsis gene *PATHOGENESIS-RELATED-1* (*PR1*), which is a hallmark of SA-dependent responses (Vlot *et al.*, 2009, Ward *et al.*, 1991). Expression of RipAY-GFP significantly reduced the SA-induced accumulation of *NbPR1* transcripts (Figure 1c), suggesting that RipAY is able to suppress SA-dependent gene expression.

RipAY-GFP localises in the nucleus and cytoplasm in *N. benthamiana* cells

To determine the subcellular localisation of RipAY in plant cells, we transiently expressed RipAY fused to a monomeric red fluorescent protein (mRFP) tag in epidermal cells of *N. benthamiana* and observed the RFP fluorescence using confocal microscopy. As a control, we co-expressed a nuclear addressed NLS-GFP. Agrobacterium-mediated transient expression indicated a cytoplasmic and nuclear localisation of RipAY-mRFP (Figure 2 and S3). Western-blot analysis confirmed that most of the signal is associated to the full-length RipAY-mRFP fusion protein present in the observed tissues (Figure S4).

RipAY associates with plant h-type thioredoxins

In order to identify plant proteins that interact with RipAY, we expressed RipAY-GFP in *N. benthamiana* and purified the fusion protein, together with associated proteins, by immunoprecipitation using agarose beads coupled to an anti-GFP nanobody. To increase the robustness of our analysis, we also expressed RipAY-HA-StrepII and purified the fusion protein by affinity pull-down using a Superflow resin bound to Strep-Tactin. As controls, we expressed and purified GFP and GFP-HA-StrepII, respectively. The purified RipAY and associated proteins were then digested with trypsin and processed by liquid-chromatography coupled to tandem mass-spectrometry (LC-MS/MS). In several biological replicates, LC-MS/MS analysis of RipAY purifications with both tags showed abundant peptides from several members of the thioredoxin h (TRX-h) family (Table 1), while no TRX-h peptides were identified after purification of GFP or GFP-HA-StrepII. Thioredoxins are small enzymes that reduce disulfide bonds of target proteins, and have been found to regulate a variety of biological processes in plants (Gelhaye *et al.*, 2005), including immune responses (Kneeshaw *et al.*, 2014, Tada *et al.*, 2008). Members from the TRX-h family are mostly considered cytosolic proteins, although membrane and nuclear localization has also been demonstrated in specific cases (Delorme-Hinoux *et al.*, 2016, Gelhaye *et al.*, 2005). To confirm this finding, we selected the four NbTRX-h proteins identified by LC-MS/MS and their closest paralogs (Figure S5) and co-expressed them, fused to a C-terminal FLAG tag, together with RipAY-GFP. GFP immunoprecipitation assays indicated that all NbTRX-h tested associated *in planta* with RipAY-GFP, but not with GFP alone used as a control (Figure 3a).

To determine whether RipAY interaction is extended to TRX-h from other plant species, we co-expressed RipAY-GFP together with five different TRX-h proteins from Arabidopsis (AtTRX-h1-5) in *N. benthamiana*. GFP immunoprecipitation assays indicated that AtTRX-h1 and AtTRX-h5 interact with RipAY-GFP (Figure 3b). AtTRX-

h1 is the most similar to the NbTRX-h proteins tested (Figure S5), and showed a stronger interaction with RipAY compared to AtTRX-h5 (Figure 3b). It is noteworthy that we occasionally detected weaker interactions with AtTRX-h3 and AtTRX-h4 (data not shown). Interestingly, AtTRX-h5 plays an important role in the regulation of immune responses, predominantly through the redox regulation of the SA-dependent transcriptional co-activator NPR1 (Kneeshaw et al., 2014, Tada et al., 2008). The expression of TRX-h5 is upregulated by flg22, SA and pathogen infection (Laloi et al., 2004, Reichheld et al., 2002, Tada et al., 2008), and *trxh5* mutants have compromised *PR1* expression after SA treatment and compromised systemic acquired resistance (SAR) (Tada et al., 2008).

RipAY cysteine is not a target of Thioredoxin redox regulation

Plant proteins that associate with pathogen effectors are usually considered virulence targets, but they can also contribute to the activation of effector activities by different mechanisms (Win et al., 2012). Considering that TRXs generally modulate the redox status of target proteins by reducing disulphide bonds in target cysteine residues, we explored whether this is the case for the interaction between TRX-h proteins and RipAY. Preliminary sequence analysis suggests that RipAY is not susceptible to reduction of intramolecular disulfide bonds, since it has only one cysteine residue (C333; Figure S6). Accordingly, mutation of C333 to a serine (C333S) did not affect the RipAY suppression of flg22-triggered ROS burst (Figure 4a), and RipAY C333S retained the ability to associate with TRXs in co-immunoprecipitation assays (Figure 4b). These results suggest that the interaction between RipAY and TRXs is not based on intramolecular or intermolecular disulphide bond reduction.

Thioredoxins as potential targets of RipAY virulence activities

To investigate whether h-type TRXs regulate immune responses in *N. benthamiana*, we employed a genetic approach based on virus-induced gene silencing (VIGS) or overexpression of different *NbTRX-h* genes. We designed two different silencing constructs, which targeted different groups of genes for silencing: the NbTRX-h9si construct is designed to target *NbTRX-h9* and *NbTRX-h11*, while the NbTRX-h15si construct is designed to target *NbTRX-h15*, *NbTRX-h10* and *NbTRX-h16* (Figure S7a). Transient expression of the mentioned silencing constructs in 3 week-old *N. benthamiana* plants led to a reduction on the mRNA levels of the corresponding *NbTRX-h* genes in younger leaves 20 days after infiltration (Figure S7b). Strikingly, while plants expressing the TRX-h15si construct showed a slight decrease in flg22-

triggered ROS, plants expressing the TRX-h9si construct displayed an enhanced ROS burst after elicitor treatment (Figure S7c). These results may be due to different roles of the different TRX-h proteins, although RipAY associated with all of them (Figure 3a), or to pleiotropic effects on additional TRXs or other redox regulators caused by the silencing of the selected *TRX-h* genes.

Overexpression of the different *NbTRX-h* genes from a cauliflower mosaic virus 35S promoter (generating NbTRX-h-FLAG fusion proteins) did not cause significant differences in flg22-triggered ROS (Figure S8a). However, the overexpression of several *NbTRX-h* genes partially rescued the inhibition of flg22-triggered ROS caused by RipAY (Figure S8b), suggesting that h-type TRXs are associated to the virulence activity of RipAY.

Since RipAY associates with AtTRX-h5 (Figure 3b) and this protein is required for several immune responses (including PR1 expression and SAR; Tada et al., 2008), we tested whether an AtTRX-h5 loss-of-function mutant (*Attrxh5-4*; Sweat & Wolpert, 2007) is also impaired in flg22-triggered ROS burst, since this response is clearly inhibited by RipAY (Figure 1). However, flg22-triggered ROS in *Attrxh5-4* showed a pattern similar to Col-0 wild-type plants (Figure S9). This suggests that additional TRXs may contribute to the regulation of flg22-triggered ROS burst, or that RipAY may additionally target other plant proteins to suppress elicitor-induced responses.

RipAY displays GGCT activity to degrade glutathione *in planta*

RipAY has no overall sequence similarity with other proteins from any organism, including plants or other plant pathogens. However, a search in the NCBI conserved domain database (Marchler-Bauer et al., 2015) indicates that RipAY central region (amino acids 126 to 252; E value = 1.65e-05; Figure S6) is similar to proteins from the gamma-glutamyl cyclotransferase (GGCT)-like superfamily, associated to the degradation of glutathione in multitude of organisms, including plants (Kumar et al., 2015, Oakley et al., 2008, Paulose et al., 2013). Therefore, we decided to test whether RipAY has an impact on the glutathione content of plant cells. One day post-infiltration (dpi) with *A. tumefaciens*, glutathione content of *N. benthamiana* tissues expressing RipAY-GFP was decreased to 30% of that of control tissues expressing GFP, despite the fact that RipAY-GFP accumulation was still very low (Figure 5a). Glutathione content decreased progressively in the following days, reaching 7.3% of that of control tissues at 3 dpi (Figure 5a). The key catalytic glutamic acid residue for GGCT activity in human and plant GGCTs is conserved in RipAY (E216; Figure S6), and mutation of this residue to glutamine has been reported to abolish GGCT activity

without altering the general protein structure (Oakley et al, 2008). Mutation of RipAY E216 to glutamine (E216Q) did not affect RipAY accumulation or the interaction with plant thioredoxins (Figure 4b), but completely abolished the RipAY-mediated decrease of plant glutathione levels (Figure 5a), indicating that the observed glutathione degradation is a product of RipAY GGCT activity.

Intriguingly, we were unable to generate Arabidopsis transgenic lines expressing RipAY, probably due to the toxicity of a sustained RipAY expression. Even the basal expression detected using a dexamethasone (DEX)-inducible construct (data not shown) prevented us from selecting RipAY-expressing plants. To determine whether RipAY is able to degrade glutathione in Arabidopsis cells, we isolated mesophyll protoplasts from Arabidopsis leaves and transfected them with a construct driving the expression of RipAY-HA-StrepII. Protoplasts expressing RipAY-HA-StrepII showed a depletion of glutathione, which required an intact E216 residue (Figure S10a). The RipAY-mediated degradation of glutathione correlated with a suppression of SA-induced accumulation of *AtPR1* transcripts (S10c), indicating that RipAY also acts as a GGCT and suppresses immune-related signalling in Arabidopsis cells.

GGCT activity is required for the suppression of immune responses

Glutathione is a master redox buffer in prokaryotes and eukaryotes, and plays a major role in plant redox homeostasis (Noctor *et al.*, 2012, Noctor *et al.*, 2011). Interestingly, glutathione is essential for the regulation of plant responses to environmental stresses, including immune responses (Frendo *et al.*, 2013, Ghanta & Chattopadhyay, 2011). Considering this, we speculated that the GGCT activity could contribute to the RipAY immune-suppression activities. Indeed, the E216Q mutation suppressed the RipAY ability to inhibit flg22-triggered ROS burst (Figure 5b) and SA-induced *PR1* expression (Figure 5c and S10c), indicating that RipAY GGCT activity is essential for RipAY suppression of the tested immune responses. Interestingly, the E216Q mutation did not affect RipAY interaction with plant thioredoxins (Figure 4b).

Considering the dramatic impact of RipAY in plant glutathione contents and flg22-triggered ROS burst (Figures 1 and 5), we decided to test whether a plant mutant with low glutathione content displays a similar inhibition of flg22-triggered ROS. The *pad2-1* mutant accumulates approximately 20% of glutathione compared to wild-type plants, and is affected in several immune responses (Dubreuil-Maurizi & Poinssot, 2012). Strikingly, we did not detect differences in the flg22-triggered ROS burst in *pad2-1* mutants compared to Col-0 wild-type plants (Figure S11a). Moreover, the

pad2-1 mutation did not cause a robust increase in the development of disease symptoms caused by *R. solanacearum* infection (Figure S11b). As an alternative chemical approach to detect the effect of glutathione depletion in immune responses, we treated *N. benthamiana* tissues with 1-chloro-2,4-dinitrobenzene (CDNB), which has been shown to decrease glutathione contents in plant cells (Okuma et al, 2011). Treatment with increasing CDNB concentrations resulted in a reduction in glutathione content, which correlated with a reduction in flg22-triggered ROS burst (Figure S11), supporting the notion that a decrease in glutathione concentration causes an inhibition of the plant response to elicitors.

DISCUSSION

Redox regulation plays an important role in plant responses to biotic and abiotic stress (Spoel & Loake, 2011, Suzuki *et al.*, 2011). Therefore, the manipulation of redox regulators may constitute a powerful tool for pathogens to subvert plant immune responses and have a broad impact on plant stress signalling. In this work, we found that the expression of the *R. solanacearum* T3E RipAY in plant cells leads to a suppression of elicitor and SA-triggered immune responses. Further biochemical analysis showed that RipAY degrades glutathione in plant cells. Glutathione is a master redox buffer (Noctor *et al.*, 2012, Noctor *et al.*, 2011), which contributes to the activation of diverse immune responses (Frendo *et al.*, 2013, Ghanta & Chattopadhyay, 2011). RipAY immune-suppression activities are abolished in a mutant on the catalytic core of the GGCT activity, which cannot degrade glutathione. This points at the degradation of glutathione as an important virulence activity of RipAY towards the suppression of immune responses. Similarly, we show that chemical depletion of glutathione in plant cells leads to a suppression of elicitor-triggered immune responses. This is consistent with previous reports showing a major contribution of glutathione to plant defence responses. For instance, the *pad2-1* mutant (deficient in glutathione biosynthesis) is impaired in the accumulation of camalexin, glucosinolates, and SA, and has deficient SA-dependent responses, including PR1 expression (Dubreuil-Maurizi & Poinssot, 2012). Also, *pad2* mutant plants are impaired in flg22-triggered callose deposition (Clay *et al.*, 2009) and are more susceptible to a wide range of pathogens and pests (Dubreuil-Maurizi & Poinssot, 2012). The association between glutathione content and plant responses to biotic stress is also supported by other reports using different glutathione-deficient mutants (Ball *et al.*, 2004). Surprisingly, in our experimental conditions, the *pad2-1* mutant was not affected in flg22-triggered ROS burst nor showed a clearly increased susceptibility to *R. solanacearum*. Considering that the GGCT activity is required for the RipAY suppression of the tested immune responses, these results suggests different possible scenarios: (i) RipAY GGCT activity may have a stronger impact on glutathione content compared to the *pad2-1* mutant; (ii) RipAY degradation of other gamma-glutamyl compounds, besides glutathione, may contribute to the observed inhibition of immune responses; (iii) a synergistic effect between glutathione degradation and the targeting of other plant proteins is required for the full virulence activity of RipAY. It is also possible that additional effects of the *pad2-1* mutation counteract the effect of glutathione deficiency, such as the reported up-regulation of *RBOHD* (Dubreuil-Maurizi *et al.*, 2011), which encodes the main NADPH oxidase

responsible for the flg22-triggered ROS burst (Nühse *et al.*, 2007, Zhang *et al.*, 2007).

RipAY associates with several h-type thioredoxins from *N. benthamiana* and Arabidopsis. H-type thioredoxins play important roles for immune responses, especially AtTRX-h5 (Kneeshaw *et al.*, 2014, Tada *et al.*, 2008), which we found to associate with RipAY in plant cells. Plant interactors can be effector targets, but may also contribute to effector activation as helpers (Win *et al.*, 2012). Therefore, we considered the possibility of TRXs acting as chaperones/helpers for RipAY, and/or contribute to activate its function. The most predominant activity described for thioredoxins consists on reducing disulfide bonds in target proteins. Targets of cytosolic thioredoxins usually have numerous Cys residues suitable for redox regulation (Ueoka-Nakanishi *et al.*, 2013). However, RipAY has only one Cys (C333; Figure S6), and we found that this Cys is not required for the interaction with thioredoxins *in planta* or for the RipAY-mediated suppression of flg22-triggered ROS burst. Moreover, the interaction between RipAY and the different TRXs tested is very strong and stable. This is in contrast with the transient interaction between TRXs and their targets, which usually can only be detected by stabilizing the interaction with a mutation in the second Cys of the TRX catalytic domain (Hisabori *et al.*, 2005). Therefore, RipAY sequence analysis and our experimental data suggest that the interaction between RipAY and thioredoxins is not based on the usual thioredoxin-mediated reduction of disulfide bonds. Additionally, we found that the overexpression of several TRXs inhibits the immune suppression activity of RipAY instead of contributing to it. This suggests that TRX overexpression could compensate for the RipAY targeting of endogenous thioredoxins, which would point to a scenario where thioredoxins are virulence targets of RipAY, or where additional redox buffering by TRXs counteracts RipAY activity.

TRXs have been postulated as effector targets based on the presence of TRX-like domains in NB-LRR proteins (integrated decoy model; Cesari *et al.*, 2014, Nishimura *et al.*, 2015). Indeed, the victorin toxin from the fungus *Cochliobolus victoriae* takes advantage of the guarding of plant TRXs by NB-LRR proteins to induce cell death in plants, which promotes disease development (Lorang *et al.*, 2012, Sweat & Wolpert, 2007). Recently, an effector from the plant-parasitic nematode *Meloidogyne javanica* has been found to manipulate the ferredoxin-thioredoxin system in root plastids, which activates ROS scavenging and suppress immune responses, enhancing susceptibility to the nematode (Lin *et al.*, 2016). Arabidopsis TRX-h5 and TRX-h3

have also been found to interact with an effector from the plant pathogenic oomycete *Hyaloperonospora arabidopsidis* (Wessling *et al.*, 2014). This suggests that pathogens from different kingdoms may have evolved to associate with plant TRXs as a general strategy to promote plant infection. Our results suggest that RipAY may affect different targets to collectively manipulate redox regulation in plant cells, leading to the suppression of immune responses (Figure S13). The reducing activities of TRXs seem to be associated to glutathione and glutathione reductases (Gelhaye *et al.*, 2004, Meyer *et al.*, 2012, Reichheld *et al.*, 2007), and TRXs and glutathione have been found to play partially overlapping roles in yeast and plants (Kovacs *et al.*, 2015, Sharma *et al.*, 2000). Therefore, it may be difficult to uncouple a potential effect of RipAY on TRXs and glutathione.

In a recent report, Fujiwara and collaborators showed that RipAY expression inhibits yeast growth, degrades glutathione, and interacts with TRXs in yeast (Fujiwara *et al.*, 2016). A detailed biochemical analysis indicated that RipAY displays a remarkably strong GGCT activity, which is required for the reported inhibition of yeast growth (Fujiwara *et al.*, 2016). Moreover, infiltration of *R. solanacearum* in eggplant leaves causes a RipAY GGCT-dependent depletion of glutathione (Fujiwara *et al.*, 2016). Interestingly, that report shows that RipAY requires the presence of eukaryotic TRXs to degrade glutathione *in vitro* and in yeast cells, and suggests that TRXs function as activators for RipAY GGCT activity. Consistent with our data *in planta*, Fujiwara *et al.* show that a redox-inactive mutant of AtTRX-h5 (C39S C42S) still interacts with RipAY, and a RipAY C333S mutant still interacts with TRXs in yeast, pointing at a redox-independent interaction between RipAY and TRXs. In light of these results, and considering that GGCT activity is essential for RipAY suppression of immune responses, we cannot not rule out the possibility that the interaction with TRXs somehow contributes to the function of RipAY via yet unknown mechanisms not based on redox regulation.

The mechanism for RipAY-mediated suppression of immunity after associating with TRXs and degrading glutathione could be related to the transcriptional co-activator NPR1. The activation and turnover of NPR1 rely on post-translational modifications, and are both required for the activation and maintenance of a subset of SA-dependent immune responses (Pajerowska-Mukhtar *et al.*, 2013, Saleh *et al.*, 2015). SA activates the reduction of the oligomeric cytosolic form of NPR1, catalysed by glutathione and TRX through disulphide reduction and denitrosylation (Kneeshaw *et al.*, 2014, Kovacs *et al.*, 2015, Mou *et al.*, 2003, Tada *et al.*, 2008). Then, the reduced

monomeric form of NPR1 translocates to the nucleus to activate the transcription of defense-related genes. RipAY targeting of redox regulators could impact NPR1 among other regulators of immune responses. Consistently, silencing of NPR1 in tomato enhances the infection by *R. solanacearum* (Chen *et al.*, 2009). Further work will be required to decipher whether the molecular mechanism of RipAY suppression of immunity is related to the redox regulation of NPR1 or other regulators of SA signalling.

The RipAY targeting of redox signalling and the suppression of immune responses could contribute to the virulence activity of RipAY in a natural infection. It is important to note that our results showing plant immune suppression by RipAY have been obtained after transient expression of RipAY in plant tissues. In a natural infection, bacteria are expected to translocate small amounts of most effector proteins, in comparison with the abundance of effector protein accumulated in plant tissues after transient expression. However, Fujiwara *et al.* (2016) have recently shown that RipAY has an extremely high catalytic activity to degrade glutathione compared to other eukaryotic GGCTs, which supports the idea that RipAY could be exerting a similar function in lower concentrations within plant cells. Consistent with this hypothesis, we failed to obtain *Arabidopsis* transgenic lines expressing RipAY, probably due to the toxicity of sustained RipAY expression, even using a plasmid containing a DEX-inducible promoter driving the expression of RipAY. This is most likely due to the residual low expression of this promoter in basal conditions, which we could observe in *N. benthamiana* (data not shown). It is noteworthy, however, that we do not detect any visible cell death during our transient expression assays (2-3 dpi) or even much later, up to 6-8 dpi, when both RipAY-GFP and the GFP-expressing control starts showing signs of chlorosis. This suggests that our results, obtained 2-3 dpi, are not a product of a general cell death phenomenon.

TRXs and glutathione have multiple targets in plant cells and regulate multiple processes besides biotic stress, such as abiotic stress and plant development (Frendo *et al.*, 2013, Gelhaye *et al.*, 2005, Ghanta & Chattopadhyay, 2011, Kneeshaw *et al.*, 2014, Noctor *et al.*, 2012, Noctor *et al.*, 2011, Tada *et al.*, 2008). Therefore, by targeting TRXs and glutathione, *R. solanacearum* could globally perturb plant signalling to benefit pathogen proliferation (Figure S13). Given the general roles of TRXs and glutathione as antioxidants (Gelhaye *et al.*, 2005, Szalai *et al.*, 2009), their manipulation could have a broader impact in the context of a natural infection, including, for example, a deficiency on ROS detoxification. Therefore, it will

be important to decipher the complex activity of RipAY in the intricate infection process by *R. solanacearum*, where the colonization of different plant organs in different stages of the infection is expected to have specific requirements in terms of manipulation of plant processes. This may also allow us to reinterpret the relevance of different plant targets for RipAY virulence activities.

When this article was in preparation, an additional report showed that RipAY is activated by thioredoxins, degrades glutathione, and suppresses elicitor-triggered responses in *N. benthamiana* (Mukaihara *et al.*, 2016). Collectively, these results, together with those published by Fujiwara and collaborators (2016), and our findings reported in this article, robustly indicate that RipAY targets redox regulators to suppress immune responses during *R. solanacearum* infection.

EXPERIMENTAL PROCEDURES

Plant material and growth conditions

N. benthamiana wild type plants were grown on soil at one plant per pot in an environmentally controlled growth room at 22°C with a 16 h photoperiod and a light-intensity of 100-150mE m⁻²s⁻¹. *A. thaliana* wild type (Col-0) and Arabidopsis mutants, *pad2-1* (Glazebrook & Ausubel, 1994) and *Attrxh5-4* (Sweat & Wolpert, 2007), were grown in a growth chamber at 22°C with a 10 h photoperiod and a light-intensity of 100-150mE m⁻²s⁻¹.

Chemicals

The flg22 peptide (TRLSSGLKINSAKDDAAGLQIA) was purchased from Abclonal, USA. Sequencing-grade modified trypsin was purchased from Promega (Madison, WI, USA). The Nanosep centrifugal filter units with Omega membrane (MWCO 10 kDa) were bought from Pall Incorporation (New York, NY, USA). All other chemicals were purchased from Sigma-Aldrich (St. Louis, MO, USA) unless otherwise stated.

Bacterial strains and cultivation conditions

Escherichia coli DH5 α was grown overnight at 37°C and 220 rpm in LB medium supplemented with appropriate antibiotics (Rifampicin 50 mg/l, Kanamycin 25 mg/l, Carbenicillin 50 mg/l, Gentamycin 25 mg/l, Spectinomycin 50 mg/l). *A. tumefaciens* strains GV3101 and GV3101(pMP90RK) were grown at 29°C and 220 rpm in LB medium supplemented with appropriate antibiotics (Rifampicin 50 mg/l, Kanamycin 25 mg/l, Carbenicillin 50 mg/l, Gentamycin 25 mg/l, Spectinomycin 50 mg/l). *R. solanacearum* GMI1000 strain was cultivated over-night in rich medium (Plener *et al.*, 2010).

RNA isolation, cDNA amplification and qRT-PCR

Total RNA was extracted using the E.Z.N.A. Plant RNA kit with DNA digestion on column (Biotek, China) according to the manufacturer's instructions. RNA samples were quantified with a Nanodrop spectrophotometer (Thermo Scientific). First strand cDNA was synthesized using the iScriptTM cDNA synthesis kit (Biorad). The open reading frames (ORFs) of thioredoxins were amplified from the first strand cDNA using the Q5 Hot Start High-Fidelity DNA polymerase (New England Biolabs). qRT-PCR was performed using the iTaqTM Universal SYBR Green Supermix (Biorad) and CFX96 Real-time system (Biorad) and the qPCR data was analyzed as described by

(Livak & Schmittgen, 2001). Primers used for cDNA amplification and qPCR are listed in Table S1.

Plasmids

The gene fragments amplified were cloned into the pENTR-D-TOPO or pDONR207 vectors (Life technologies) and then sub-cloned into different gateway binary vectors via LR reactions (Life technologies). The *RipAY* (*Rsp1022*) gene from the *R. solanacearum* *GMI1000* strain (pACC384, pDONR207 base) and *RipAY* mutants were subcloned into pGWB505 (Nakagawa *et al.*, 2007) to generate a C-terminal fusion with an eGFP tag, and pXCSG-HAStrep (Witte *et al.*, 2004) to generate a C-terminal fusion with a HA-StrepII tag. The amplified ORF of thioredoxins were subcloned into pGWB511 (Nakagawa *et al.*, 2007) carrying 3-terminal sequence encoding flag tag. pGWB constructs were transformed into *A. tumefaciens* *GV3101*, while pXCSG-HAStrep constructs were transformed into *A. tumefaciens* *GV3101* (*pMMP90RK*). The *RipAY*-mRFP construct was generated by LR recombination of the *RipAY* ENTRY clone (pACC384, pDONR207 base), with the pDEST binary vector pGR0029RFP2 (Deslandes *et al.*, 2003). The NLS-GFP construct was generated by LR recombination of an NLS SV40 pENTRY clone (pNP50, pENTR sd/d/topo base) into the pDEST binary vector pMDC83 (Curtis & Grossniklaus, 2003).

Agrobacterium-mediated transient expression

Agrobacterium-mediated transient expression in *N. benthamiana* was performed as described (Li, 2011). Before infiltration, the bacterial suspension was adjusted to a final OD₆₀₀ of 0.5. Samples were taken at 1-3 dpi (days post infiltration) for analysis based on experimental requirements.

Measurement of ROS generation

Oxidative burst measurements were performed as described previously (Gimenez-Ibanez *et al.*, 2009), with some modifications. ROS were elicited with 50nM flg22, and the luminescence was measured over 60 min using a Microplate luminescence reader (Varioskan flash, Thermo Scientific, USA). The luminescence was recorded in each well during 400 milliseconds every minute over 60 minutes. The data obtained from the ROS burst assay was analyzed and represented in two different ways, showing the relative luminescence units (RLU) produced per minute (representing the kinetics of ROS production in different samples over 60 minutes), and the total accumulative values of RLU for each sample (representing the total ROS production in different samples over the duration of the assay).

MAPK activation

MAPK activation assays were performed using 4 to 5-week-old *N. benthamiana* as described previously (Segonzac *et al.*, 2011) with several modifications. Two days after *Agrobacterium* infiltration, four 8 mm-diameter leaf discs were taken from infiltrated leaves and frozen in liquid nitrogen as negative control. The rest of the leaves were then elicited for 15 min after vacuum infiltration of 100 nM flg22 and samples were taken and frozen in liquid nitrogen. MAPK activation was monitored by western blot with Phospho-p44/42 MAPK (Erk1/2; Thr-202/Tyr-204) antibodies from Cell Signaling according to the manufacturer's protocol. Blots were stained with Coomassie Brilliant Blue to verify equal loading.

Confocal microscopy

Confocal laser scanning microscopy was performed, using a Leica AOBs confocal microscope using the abaxial side of *Agrobacterium*-infiltrated *N. benthamiana* leaves. Leaves were observed from 24 to 48 h post-infiltration. After co-transformation of plant cells with RipAY-mRFP and NLS-GFP, both red and green channels were recorded, signal saturation was avoided, and several fields of view were inspected to have a global overview of the putative localisation of RipAY-mRFP.

Measurements of total cellular glutathione in *N. benthamiana* leaves

Total cellular glutathione was measured using the Glutathione Assay Kit (Sigma-Aldrich) according to the manufacturer's instructions. Briefly, 100 mg leaf tissues were collected and frozen in liquid nitrogen at 1, 2 and 3 dpi, respectively. The frozen tissues were ground with a tissuelyser (Qiagen) and 1.0 ml of 5% 5-Sulfosalicylic acid was added to the powder to extract total glutathione. After centrifugation, 10 μ l of the supernatant were used for glutathione measurement, which was then normalized to the weight of the original sample used.

Site-directed mutagenesis

RipAY-E216Q and RipAY-C333S mutant variants were generated using the QuickChange lightning Site-Directed Mutagenesis Kit (Life technologies, USA) following the manufacturer's instructions. RipAY/pDONR207 plasmid was used as template and the primers used for the mutagenesis are listed in Table S1.

Infections with *Ralstonia solanacearum*

Four week-old *A. thaliana* plants, grown in Jiffy pods, were inoculated, without wounding, by soil drenching. An overnight-grown bacterial suspension was diluted to obtain an inoculum of $5 \cdot 10^7$ cfu/ml. Typically a 2 L inoculum was used to soak up to 50 *A. thaliana* containing Jiffy pods. Once the Jiffy pods were completely drenched (after approximately 10 min) the plants were removed from the bacterial solution and placed back on a bed of potting mixture soil, in the same original inoculation tray. The genotypes to be tested (here Col-0 versus *pad2-1*) were placed in a predefined random order in order to allow an unbiased analysis of the wilting. Three real biological repetitions were performed (each inoculated with a separate GMI1000 inoculum), with each repetition containing 17 Col-0 and 16 *pad2-1* plants. Daily scoring of the visible wilting on a scale ranging from 0 to 4 (or 0 to 100% leaves wilting), led to an analysis using the Kaplan-Meier survival analysis, log-rank test and hazard ratio calculation as previously described (Remigi *et al.*, 2011, Wang *et al.*, 2015).

Large-scale immunoprecipitation assays for LC-MS/MS analysis

Large-scale immunoprecipitation assays for LC-MS/MS analysis were performed as previously described (Kadota *et al.*, 2016), with several modifications. Three to five grams of *N. benthamiana* leaf materials at 2 dpi were frozen and ground in liquid nitrogen. Total proteins were extracted using protein extraction buffer (100 mM Tris-HCl pH7.5, 150 mM NaCl, 10% glycerol, 5 mM EDTA, 10 mM DTT, 2 mM PMSF, 10 mM NaF, 10 mM Na_2MoO_4 , 2 mM NaVO_3 , 0.5%(v/v) IGEPAL, 1%(v/v) Plant Protease Inhibitor cocktail (Sigma). To use step-tactin beads, 100 ug/ml avidin was included in the protein extraction buffer. Extracts were centrifuged twice at 15,000 g for 15 minutes at 4°C to remove the debris completely. GFP-trap beads (ChromoTek, Germany) or strep-tactin beads (IBA-lifesciences, Germany) were added into the supernatant and incubated for one hour at 4 °C with slow but constant rotation. Conjugated beads were washed three times with 1 ml cold wash buffer (100 mM Tris-HCl pH7.5, 150 mM NaCl, 10% glycerol, 2 mM DTT, 10 mM NaF, 10 mM Na_2MoO_4 , 2 mM NaVO_3 , 0.5%(v/v) IGEPAL, 1%(v/v) Plant Protease Inhibitor cocktail (Sigma)) and twice with wash buffer without IGEPAL before stripping interacting proteins from the beads by boiling in 50 ul Laemmli sample buffer (Biorad) for 10 minutes. Immunoprecipitated proteins were separated on precast SDS-PAGE gels (Biorad). Gels were washed five times with MilliQ water (Millipore, USA) and stained with Commassie Brilliant Blue G250 (Biorad) for 1 h. The stained gel was destained twice with MilliQ water and cut into pieces for protein identification.

Co-immunoprecipitation

N. benthamiana leaves were co-infiltrated with *A. tumefaciens* GV3101 carrying plasmids to induce the expression of RipAY-GFP (pGWB505) and TRX-h-FLAG (pGWB511). Leaves infiltrated with GV3101 carrying the GFP (pGWB505) and TRX-h-FLAG (pGWB511) were used as negative control. After 2 dpi, total proteins were extracted and immunoprecipitation was performed with GFP-trap beads as described above, except that the conjugated beads were washed five times with 1 ml cold wash buffer with IGEPAL before stripping interacting proteins from the beads by boiling in 50 μ l SDS loading buffer for 10 minutes. The immunoprecipitated proteins were separated on SDS-PAGE gels and Western blot was performed using the anti-FLAG (Sigma) and anti-GFP (Abiocode) primary antibodies, respectively. Blots were stained with Coomassie Brilliant Blue to verify equal loading.

Protein digestion, LC-MS/MS analysis and protein identification

Detailed information about protein digestion, liquid-chromatography coupled to tandem mass-spectrometric analysis and protein identification can be found in the Supporting Information.

Virus-induced gene silencing (VIGS) of thioredoxins in *N. benthamiana*

VIGS was performed using TRV vectors as described (Senthil-Kumar & Mysore, 2014). Silencing fragments of NbTrx09/11 (NbTRX-h9si) and NbTrx10/15/16 (NbTRX-h15si) were amplified, respectively, using the primers listed in Table 1, and cloned into pEASY vectors (Transgene, China). After digestion with EcoRI and XhoI (New England Biolabs), the silencing fragments were sub-cloned into TRV2 vectors to make the TRV2:NbTRX-h9 and TRV2:NbTRX-h15 silencing constructs. These constructs were transformed into *A. tumefaciens* GV3101 for agroinfiltration in the lower leaves of 3 week-old *N. benthamiana* plants.

ACKNOWLEDGEMENTS

We thank Rosa Lozano-Durán for critical reading and suggestions to this manuscript. We also thank members of the Macho and Lozano-Durán laboratories for helpful discussions, and Xinyu Jian for technical and administrative assistance during this work. We thank Laurent Noël, Thomas Wolpert and Benoît Poinssot for sharing biological materials. We are grateful to Cécile Pouzet and Aurélie Le Ru of the T.R.I. GENOTOUL microscopy platform (FRAIB, Toulouse, France) for performing confocal imaging. Research in the Macho laboratory is supported by the Shanghai Center for Plant Stress Biology (Chinese Academy of Sciences), National Natural Science Foundation of China (grant 31571973) and the Chinese 1000 Talents Program. ACC and NP are supported by the LABEX TULIP (ANR-10-LABX-41 and ANR-11-IDEX-0002-02).

REFERENCES

- Ball, L., Accotto, G. P., Bechtold, U., Creissen, G., Funck, D., Jimenez, A., *et al.* (2004) Evidence for a direct link between glutathione biosynthesis and stress defense gene expression in Arabidopsis. *Plant Cell*, **16**, 2448-2462.
- Bigeard, J., Colcombet, J. and Hirt, H. (2015) Signaling mechanisms in pattern-triggered immunity (PTI). *Mol Plant*, **8**, 521-539.
- Boller, T. and Felix, G. (2009) A renaissance of elicitors: perception of microbe-associated molecular patterns and danger signals by pattern-recognition receptors. *Annu Rev Plant Biol*, **60**, 379-406.
- Cesari, S., Bernoux, M., Moncuquet, P., Kroj, T. and Dodds, P. N. (2014) A novel conserved mechanism for plant NLR protein pairs: the "integrated decoy" hypothesis. *Front Plant Sci*, **5**, 606.
- Chen, Y. Y., Lin, Y. M., Chao, T. C., Wang, J. F., Liu, A. C., Ho, F. I., *et al.* (2009) Virus-induced gene silencing reveals the involvement of ethylene-, salicylic acid- and mitogen-activated protein kinase-related defense pathways in the resistance of tomato to bacterial wilt. *Physiol Plantarum*, **136**, 324-335.
- Clarke, C. R., Studholme, D. J., Hayes, B., Runde, B., Weisberg, A., Cai, R., *et al.* (2015) Genome-Enabled Phylogeographic Investigation of the Quarantine Pathogen *Ralstonia solanacearum* Race 3 Biovar 2 and Screening for Sources of Resistance Against Its Core Effectors. *Phytopathology*, **105**, 597-607.
- Clay, N. K., Adio, A. M., Denoux, C., Jander, G. and Ausubel, F. M. (2009) Glucosinolate metabolites required for an Arabidopsis innate immune response. *Science*, **323**, 95-101.
- Cook, D. E., Mesarich, C. H. and Thomma, B. P. (2015) Understanding plant immunity as a surveillance system to detect invasion. *Annu Rev Phytopathol*, **53**, 541-563.
- Curtis, M. D. and Grossniklaus, U. (2003) A gateway cloning vector set for high-throughput functional analysis of genes in planta. *Plant Physiol*, **133**, 462-469.
- Delorme-Hinoux, V., Bangash, S. A., Meyer, A. J. and Reichheld, J. P. (2016) Nuclear thiol redox systems in plants. *Plant Sci*, **243**, 84-95.
- Deslandes, L. and Genin, S. (2014) Opening the *Ralstonia solanacearum* type III effector tool box: insights into host cell subversion mechanisms. *Curr Opin Plant Biol*, **20**, 110-117.
- Deslandes, L., Olivier, J., Peeters, N., Feng, D. X., Khounloham, M., Boucher, C., *et al.* (2003) Physical interaction between RRS1-R, a protein conferring resistance to bacterial wilt, and PopP2, a type III effector targeted to the plant nucleus. *Proc Natl Acad Sci U S A*, **100**, 8024-8029.
- Deslandes, L. and Rivas, S. (2012) Catch me if you can: bacterial effectors and plant targets. *Trends Plant Sci*, **17**, 644-655.
- Dubreuil-Maurizi, C. and Poinssot, B. (2012) Role of glutathione in plant signaling under biotic stress. *Plant Signal Behav*, **7**, 210-212.
- Dubreuil-Maurizi, C., Vitecek, J., Marty, L., Branciard, L., Frettinger, P., Wendehenne, D., *et al.* (2011) Glutathione deficiency of the Arabidopsis mutant pad2-1 affects oxidative stress-related events, defense gene expression, and the hypersensitive response. *Plant Physiol*, **157**, 2000-2012.
- Frendo, P., Baldacci-Cresp, F., Benyamina, S. M. and Puppo, A. (2013) Glutathione and plant response to the biotic environment. *Free Radic Biol Med*, **65**, 724-730.
- Fujiwara, S., Kawazoe, T., Ohnishi, K., Kitagawa, T., Popa, C., Valls, M., *et al.* (2016) RipAY, a Plant Pathogen Effector Protein, Exhibits Robust gamma-Glutamyl Cyclotransferase Activity When Stimulated by Eukaryotic Thioredoxins. *J Biol Chem*, **291**, 6813-6830.
- Galan, J. E., Lara-Tejero, M., Marlovits, T. C. and Wagner, S. (2014) Bacterial Type III Secretion Systems: Specialized Nanomachines for Protein Delivery into Target Cells. *Annu Rev Microbiol*, **68**, 415-438.
- Gelhaye, E., Rouhier, N. and Jacquot, J. P. (2004) The thioredoxin h system of higher plants. *Plant physiology and biochemistry : PPB / Societe francaise de physiologie vegetale*, **42**, 265-271.
- Gelhaye, E., Rouhier, N., Navrot, N. and Jacquot, J. P. (2005) The plant thioredoxin system. *Cell Mol Life Sci*, **62**, 24-35.

- Ghanta, S. and Chattopadhyay, S. (2011) Glutathione as a signaling molecule: another challenge to pathogens. *Plant Signal Behav*, **6**, 783-788.
- Gimenez-Ibanez, S., Hann, D. R., Ntoukakis, V., Petutschnig, E., Lipka, V. and Rathjen, J. P. (2009) AvrPtoB targets the LysM receptor kinase CERK1 to promote bacterial virulence on plants. *Curr Biol*, **19**, 423-429.
- Glazebrook, J. and Ausubel, F. M. (1994) Isolation of phytoalexin-deficient mutants of *Arabidopsis thaliana* and characterization of their interactions with bacterial pathogens. *Proc Natl Acad Sci U S A*, **91**, 8955-8959.
- Gómez-Gómez, L. and Boller, T. (2000) FLS2: an LRR receptor-like kinase involved in the perception of the bacterial elicitor flagellin in *Arabidopsis*. *Mol Cell*, **5**, 1003-1011.
- Hisabori, T., Hara, S., Fujii, T., Yamazaki, D., Hosoya-Matsuda, N. and Motohashi, K. (2005) Thioredoxin affinity chromatography: a useful method for further understanding the thioredoxin network. *J Exp Bot*, **56**, 1463-1468.
- Jones, J. D. and Dangl, J. L. (2006) The plant immune system. *Nature*, **444**, 323-329.
- Kadota, Y., Macho, A. P. and Zipfel, C. (2016) Immunoprecipitation of Plasma Membrane Receptor-Like Kinases for Identification of Phosphorylation Sites and Associated Proteins. *Methods Mol Biol*, **1363**, 133-144.
- Khan, M., Subramaniam, R. and Desveaux, D. (2016) Of guards, decoys, baits and traps: pathogen perception in plants by type III effector sensors. *Curr Opin Microbiol*, **29**, 49-55.
- Kneeshaw, S., Gelineau, S., Tada, Y., Loake, G. J. and Spoel, S. H. (2014) Selective protein denitrosylation activity of Thioredoxin-h5 modulates plant Immunity. *Mol Cell*, **56**, 153-162.
- Kovacs, I., Durner, J. and Lindermayr, C. (2015) Crosstalk between nitric oxide and glutathione is required for NONEXPRESSOR OF PATHOGENESIS-RELATED GENES 1 (NPR1)-dependent defense signaling in *Arabidopsis thaliana*. *New Phytol*, **208**, 860-872.
- Kumar, S., Kaur, A., Chattopadhyay, B. and Bachhawat, A. K. (2015) Defining the cytosolic pathway of glutathione degradation in *Arabidopsis thaliana*: role of the ChaC/GCG family of gamma-glutamyl cyclotransferases as glutathione-degrading enzymes and AtLAP1 as the Cys-Gly peptidase. *Biochem J*, **468**, 73-85.
- Laloi, C., Mestres-Ortega, D., Marco, Y., Meyer, Y. and Reichheld, J. P. (2004) The *Arabidopsis* cytosolic thioredoxin h5 gene induction by oxidative stress and its W-box-mediated response to pathogen elicitor. *Plant Physiol*, **134**, 1006-1016.
- Li, X. (2011) Infiltration of *Nicotiana benthamiana* Protocol for Transient Expression via *Agrobacterium*. *Bio-protocol*, **Bio101**.
- Lin, B., Zhuo, K., Chen, S., Hu, L., Sun, L., Wang, X., *et al.* (2016) A novel nematode effector suppresses plant immunity by activating host reactive oxygen species-scavenging system. *New Phytol*, **209**, 1159-1173.
- Livak, K. J. and Schmittgen, T. D. (2001) Analysis of relative gene expression data using real-time quantitative PCR and the 2(-Delta Delta C) method. *Methods*, **25**, 402-408.
- Lorang, J., Kidarsa, T., Bradford, C. S., Gilbert, B., Curtis, M., Tzeng, S. C., *et al.* (2012) Tricking the guard: exploiting plant defense for disease susceptibility. *Science*, **338**, 659-662.
- Macho, A. P. (2016) Subversion of plant cellular functions by bacterial type-III effectors: beyond suppression of immunity. *New Phytol*, **210**, 51-57.
- Macho, A. P., Guidot, A., Barberis, P., Beuzon, C. R. and Genin, S. (2010) A competitive index assay identifies several *Ralstonia solanacearum* type III effector mutant strains with reduced fitness in host plants. *Mol Plant Microbe Interact*, **23**, 1197-1205.
- Macho, A. P. and Zipfel, C. (2014) Plant PRRs and the Activation of Innate Immune Signaling. *Mol Cell*, **54**, 263-272.
- Macho, A. P. and Zipfel, C. (2015) Targeting of plant pattern recognition receptor-triggered immunity by bacterial type-III secretion system effectors. *Curr Opin Microbiol*, **23C**, 14-22.
- Mansfield, J., Genin, S., Magori, S., Citovsky, V., Sriariyanum, M., Ronald, P., *et al.* (2012) Top 10 plant pathogenic bacteria in molecular plant pathology. *Mol Plant Pathol*, **13**, 614-629.
- Marchler-Bauer, A., Derbyshire, M. K., Gonzales, N. R., Lu, S., Chitsaz, F., Geer, L. Y., *et al.* (2015) CDD: NCBI's conserved domain database. *Nucleic acids research*, **43**, D222-226.

- Meyer, Y., Belin, C., Delorme-Hinoux, V., Reichheld, J. P. and Riondet, C. (2012) Thioredoxin and Glutaredoxin Systems in Plants: Molecular Mechanisms, Crosstalks, and Functional Significance. *Antioxid Redox Sign*, **17**, 1124-1160.
- Monteiro, F., Genin, S., van Dijk, I. and Valls, M. (2012) A luminescent reporter evidences active expression of *Ralstonia solanacearum* type III secretion system genes throughout plant infection. *Microbiol*, **158**, 2107-2116.
- Mou, Z., Fan, W. and Dong, X. (2003) Inducers of plant systemic acquired resistance regulate NPR1 function through redox changes. *Cell*, **113**, 935-944.
- Mukaihara, T., Hatanaka, T., Nakano, M. and Oda, K. (2016) *Ralstonia solanacearum* type III effector RipAY is a glutathione-degrading enzyme that is activated by plant cytosolic thioredoxins and suppresses plant immunity. *mBio*, **7**, e00359-16.
- Nakagawa, T., Suzuki, T., Murata, S., Nakamura, S., Hino, T., Maeo, K., *et al.* (2007) Improved Gateway binary vectors: high-performance vectors for creation of fusion constructs in transgenic analysis of plants. *Biosci Biotechnol Biochem*, **71**, 2095-2100.
- Nishimura, M. T., Monteiro, F. and Dangl, J. L. (2015) Treasure your exceptions: unusual domains in immune receptors reveal host virulence targets. *Cell*, **161**, 957-960.
- Noctor, G., Mhamdi, A., Chaouch, S., Han, Y., Neukermans, J., Marquez-Garcia, B., *et al.* (2012) Glutathione in plants: an integrated overview. *Plant Cell Environ*, **35**, 454-484.
- Noctor, G., Queval, G., Mhamdi, A., Chaouch, S. and Foyer, C. H. (2011) Glutathione. *Arabidopsis Book*, **9**, e0142.
- Nühse, T. S., Bottrill, A. R., Jones, A. M. E. and Peck, S. C. (2007) Quantitative phosphoproteomic analysis of plasma membrane proteins reveals regulatory mechanisms of plant innate immune responses. *Plant J* **51**, 931-940.
- Oakley, A. J., Yamada, T., Liu, D., Coggan, M., Clark, A. G. and Board, P. G. (2008) The identification and structural characterization of C7orf24 as gamma-glutamyl cyclotransferase. An essential enzyme in the gamma-glutamyl cycle. *J Biol Chem*, **283**, 22031-22042.
- Okuma, E., Sarwar-Jahan, M.D., Munemasa, S., Anowar-Hossain, M., Muroyama, D., Mahub-Islam, M., *et al.* (2011) Negative regulation of abscisic acid-induced stomatal closure by glutathione in Arabidopsis. *J Plant Physiol*, **168**, 2048-2055.
- Pajerowska-Mukhtar, K. M., Emerine, D. K. and Mukhtar, M. S. (2013) Tell me more: roles of NPRs in plant immunity. *Trends Plant Sci*, **18**, 402-411.
- Paulose, B., Chhikara, S., Coomey, J., Jung, H. I., Vatamaniuk, O. and Dhankher, O. P. (2013) A gamma-glutamyl cyclotransferase protects Arabidopsis plants from heavy metal toxicity by recycling glutamate to maintain glutathione homeostasis. *Plant Cell*, **25**, 4580-4595.
- Peeters, N., Carrere, S., Anisimova, M., Plener, L., Cazale, A. C. and Genin, S. (2013a) Repertoire, unified nomenclature and evolution of the Type III effector gene set in the *Ralstonia solanacearum* species complex. *BMC genomics*, **14**, 859.
- Peeters, N., Guidot, A., Vailleau, F. and Valls, M. (2013b) *Ralstonia solanacearum*, a widespread bacterial plant pathogen in the post-genomic era. *Mol Plant Pathol*, **14**, 651-662.
- Plener, L., Manfredi, P., Valls, M. and Genin, S. (2010) PrhG, a transcriptional regulator responding to growth conditions, is involved in the control of the type III secretion system regulon in *Ralstonia solanacearum*. *J Bacteriol*, **192**, 1011-1019.
- Reichheld, J. P., Khafif, M., Riondet, C., Droux, M., Bonnard, G. and Meyer, Y. (2007) Inactivation of thioredoxin reductases reveals a complex interplay between thioredoxin and glutathione pathways in Arabidopsis development. *Plant Cell*, **19**, 1851-1865.
- Reichheld, J. P., Mestres-Ortega, D., Laloi, C. and Meyer, Y. (2002) The multigenic family of thioredoxin h in Arabidopsis thaliana: specific expression and stress response. *Plant Physiol Bioch*, **40**, 685-690.
- Remigi, P., Anisimova, M., Guidot, A., Genin, S. and Peeters, N. (2011) Functional diversification of the GALA type III effector family contributes to *Ralstonia solanacearum* adaptation on different plant hosts. *New Phytol*, **192**, 976-987.
- Saleh, A., Withers, J., Mohan, R., Marques, J., Gu, Y., Yan, S., *et al.* (2015) Posttranslational Modifications of the Master Transcriptional Regulator NPR1 Enable Dynamic but Tight Control of Plant Immune Responses. *Cell Host Microbe*, **18**, 169-182.

- Segonzac, C., Feike, D., Gimenez-Ibanez, S., Hann, D. R., Zipfel, C. and Rathjen, J. P. (2011) Hierarchy and Roles of Pathogen-Associated Molecular Pattern-Induced Responses in *Nicotiana benthamiana*. *Plant Physiol*, **156**, 687-699.
- Senthil-Kumar, M. and Mysore, K. S. (2014) Tobacco rattle virus-based virus-induced gene silencing in *Nicotiana benthamiana*. *Nat Protoc*, **9**, 1549-1562.
- Sharma, K. G., Sharma, V., Bourbonloux, A., Delrot, S. and Bachhawat, A. K. (2000) Glutathione depletion leads to delayed growth stasis in *Saccharomyces cerevisiae*: evidence of a partially overlapping role for thioredoxin. *Curr Genet*, **38**, 71-77.
- Spoel, S. H. and Loake, G. J. (2011) Redox-based protein modifications: the missing link in plant immune signalling. *Curr Opin Plant Biol*, **14**, 358-364.
- Sun, Y., Li, L., Macho, A. P., Han, Z., Hu, Z., Zipfel, C., *et al.* (2013) Structural basis for flg22-induced activation of the Arabidopsis FLS2-BAK1 immune complex. *Science*, **342**, 624-628.
- Suzuki, N., KOUSSEVITZKY, S., Mittler, R. and Miller, G. (2011) ROS and redox signalling in the response of plants to abiotic stress. *Plant, Cell & Environment*, **35**, 259-270.
- Sweat, T. A. and Wolpert, T. J. (2007) Thioredoxin h5 is required for victorin sensitivity mediated by a CC-NBS-LRR gene in Arabidopsis. *Plant Cell*, **19**, 673-687.
- Szalai, G., Kellos, T., Galiba, G. and Kocsy, G. (2009) Glutathione as an Antioxidant and Regulatory Molecule in Plants Under Abiotic Stress Conditions. *J Plant Growth Regul*, **28**, 66-80.
- Tada, Y., Spoel, S. H., Pajerowska-Mukhtar, K., Mou, Z., Song, J., Wang, C., *et al.* (2008) Plant immunity requires conformational changes [corrected] of NPR1 via S-nitrosylation and thioredoxins. *Science*, **321**, 952-956.
- Tsuda, K. and Katagiri, F. (2010) Comparing signaling mechanisms engaged in pattern-triggered and effector-triggered immunity. *Curr Opin Plant Biol*, **13**, 459-465.
- Ueoka-Nakanishi, H., Sazuka, T., Nakanishi, Y., Maeshima, M., Mori, H. and Hisabori, T. (2013) Thioredoxin h regulates calcium dependent protein kinases in plasma membranes. *FEBS J*, **280**, 3220-3231.
- Vlot, A. C., Dempsey, D. A. and Klessig, D. F. (2009) Salicylic Acid, a multifaceted hormone to combat disease. *Annu Rev Phytopathol*, **47**, 177-206.
- Wang, K., Remigi, P., Anisimova, M., Lonjon, F., Kars, I., Kajava, A., *et al.* (2015) Functional Assignment to Positively Selected Sites in the Core Type III Effector RipG7 from *Ralstonia solanacearum*. *Mol Plant Pathol*. doi: 10.1111/mpp.12302
- Ward, E. R., Uknes, S. J., Williams, S. C., Dincher, S. S., Wiederhold, D. L., Alexander, D. C., *et al.* (1991) Coordinate Gene Activity in Response to Agents That Induce Systemic Acquired Resistance. *Plant Cell*, **3**, 1085-1094.
- Wessling, R., Epple, P., Altmann, S., He, Y., Yang, L., Henz, S. R., *et al.* (2014) Convergent targeting of a common host protein-network by pathogen effectors from three kingdoms of life. *Cell Host Microbe*, **16**, 364-375.
- Win, J., Chaparro-Garcia, A., Belhaj, K., Saunders, D. G., Yoshida, K., Dong, S., *et al.* (2012) Effector Biology of Plant-Associated Organisms: Concepts and Perspectives. *Cold Spring Harb Symp Quant Biol*. **77**, 235-47
- Witte, C. P., Noel, L. D., Gielbert, J., Parker, J. E. and Romeis, T. (2004) Rapid one-step protein purification from plant material using the eight-amino acid StrepII epitope. *Plant Mol Biol*, **55**, 135-147.
- Zhang, J., Shao, F., Li, Y., Cui, H., Chen, L., Li, H., *et al.* (2007) A *Pseudomonas syringae* Effector Inactivates MAPKs to Suppress PAMP-Induced Immunity in Plants. *Cell Host Microbe*, **1**, 175-185.
- Zipfel, C. (2014) Plant Pattern Recognition Receptors. *Trends in Immunology*, **35**, 345-51.

SUPPORTING INFORMATION LEGENDS

Supporting experimental procedures: Protein digestion, LC-MS/MS analysis and protein identification.

Figure S1. RipAY-HA-StrepII suppresses flg22-triggered ROS in *N. benthamiana* leaves.

A. tumefaciens was used to induce the transient expression of RipAY-HA-StrepII in half of the leaf and GFP-HA-StrepII in the other half. **(a, b)** Oxidative burst triggered by 50 nM flg22 in *N. benthamiana* tissues 2.5 days post-inoculation (dpi) with *A. tumefaciens*, and measured in a luminol-based assay as relative luminescence units (RLU). Values are average \pm SE (n=24). Asterisks indicate significant differences compared to the corresponding GFP control at $P < 0.001$. The experiment was repeated at least three times with similar results.

Figure S2. RipAY does not cause a clear and reproducible suppression of flg22-triggered MAPK activation.

A. tumefaciens was used to induce the transient expression of RipAY-GFP in half of the leaf and GFP in the other half. MAPK activation was induced with 100nM flg22 and analysed 15 minutes after flg22 treatment using anti-phosphorylated MAPK antibody (anti-pMAPK). Immunoblots were also analysed using anti-GFP antibody to verify protein accumulation. CBB, Coomassie Brilliant Blue. Molecular weight (kDa) marker bands are indicated for reference. The experiments were repeated three times with similar results.

Figure S3. RipAY-mRFP localizes to cytoplasmic and nuclear plant cell compartments.

Four additional independent confocal microscopy images of *N. benthamiana* epidermal cells expressing RipAY-mRFP. N: nucleus, arrows: cytoplasmic strands.

Figure S4. Western blot analysis of RipAY-mRFP.

Western blot analysis of the *N. benthamiana* tissues used to determine the subcellular localisation of RipAY-mRFP (lanes marked in red). The expected size of the RipAY-mRFP fusion protein and the free mRFP are indicated for reference. These representative experiments indicate that at least most of the signal observed under the confocal microscope is associated to the full-length RipAY-mRFP. A faint band with the expected size of free mRFP was occasionally observed, and could

correspond to the cleavage of a small proportion of the mRFP tag *in planta* or during the protein extraction process.

Figure S5. *N. benthamiana* thioredoxins studied in this work.

(a) H-type thioredoxins identified associated with RipAY, and their equivalent nomenclatures in the *N. benthamiana* genome versions (www.solgenomics.org) and this work. (b) Phylogenetic tree of the *N. benthamiana* and *A. thaliana* h-type thioredoxins studied in this work.

Figure S6. RipAY sequence analysis.

Aminoacid sequence of RipAY from *Ralstonia solanacearum* GMI1000, used in this work. The GGCT domain is underlined in red. The conserved catalytic glutamate residue (E216) is marked with a green box. The only cysteine residue (C333) is marked with a blue box.

Figure S7. Genetic analysis by silencing of *N. benthamiana* thioredoxins.

(a) Phylogenetic tree of the *N. benthamiana* h-type thioredoxins studied in this work. Two silencing constructs were generated to silence the two different groups marked with red boxes. (b) Quantitative RT-PCR analysis of *NbTRX-h* transcripts in *N. benthamiana* leaves, 20 days post-inoculation (dpi) of lower leaves with *A. tumefaciens* expressing a control construct or the different silencing constructs, as detailed in the materials and methods section. Gene expression values are relative to the *NbEF1 α* housekeeping gene and are normalized to tissues expressing the silencing control. (c) Oxidative burst was triggered by 50 nM flg22 in *N. benthamiana* tissues silenced for the different *NbTRX-h* genes, and measured in a luminol-based assay as relative luminescence units (RLU) over 60 minutes. Values are average \pm SE (n=24). Asterisks indicate significant differences compared to the corresponding VIGS control at P<0.05. The experiments were repeated at least three times with similar results.

Figure S8. Analysis of the impact of overexpression of *NbTRX-h* genes on flg22-triggered ROS burst.

(a) *A. tumefaciens* was used to induce the transient expression of different *NbTRX-h*-FLAG fusion proteins in half of the leaf and GFP in the other half. (b) *A. tumefaciens* was used to induce the transient expression of RipAY-GFP in half of the leaf and GFP in the other half, co-inoculated with *A. tumefaciens* with no plasmid or triggering the transient expression of different *NbTRX-h*-FLAG fusion proteins. Oxidative burst

triggered by 50 nM flg22 in *N. benthamiana* tissues 2.5 days post-inoculation (dpi) with *A. tumefaciens*, and measured in a luminol-based assay as relative luminescence units (RLU). Values are average \pm SE (n=24). Immunoblots were analysed using anti-GFP and anti-FLAG antibodies to verify protein accumulation. CBB, Coomassie Brilliant Blue. Asterisks indicate significant differences compared to the value obtained in control RipAY-expressing tissues at $P < 0.001$. The experiments were repeated three times with similar results.

Figure S9. The *trxh5-4* mutation does not affect the flg22-triggered ROS burst.

Oxidative burst triggered by 50 nM flg22 in wild-type Col-0 and *trxh5-4* mutant plants measured in a luminol-based assay as relative light units (RLU). Values are average \pm SE (n=24). The experiments were repeated three times with similar results.

Figure S10. RipAY degrades glutathione and suppresses SA-triggered *PR1* induction in Arabidopsis mesophyll protoplasts.

(a) Total glutathione content in Arabidopsis mesophyll protoplasts expressing GFP-HA-Strep, RipAY-HA-Strep or RipAY-E216Q-HA-Strep. Values are average \pm SE (n=3). Approximately 15000 protoplasts were used per sample. (b) Immunoblot to confirm protein accumulation in transfected protoplasts, using anti-HA. CBB, Coomassie Brilliant Blue. (c) Quantitative RT-PCR analysis of *AtPR1* transcripts in Arabidopsis mesophyll protoplasts either untreated or treated with 0.1 mM SA for 2 h. Gene expression values are relative to the *AtActin2* housekeeping gene and are normalized to untreated protoplasts. Values are average \pm SE (n=3). Asterisks indicate significant differences compared to the corresponding GFP control at $P < 0.001$. The experiments were repeated twice with similar results.

Figure S11. Analysis of flg22-triggered ROS burst and *Ralstonia solanacearum* infection in the *pad2-1* mutant.

(a) The *pad2-1* mutation does not affect the flg22-triggered ROS burst. Oxidative burst triggered by 50 nM flg22 in wild-type Col-0 and *pad2-1* mutant plants measured in a luminol-based assay as relative light units (RLU). Values are average \pm SE (n=24). The experiments were repeated three times with similar results. (b) The bacterial wilt disease provoked by *R. solanacearum* GMI1000 is not distinguishable between Col-0 and *pad2-1*. Hazard ratio representation of three biological independent inoculation experiments. The median of the three data points is represented. Using a one-tailed paired t-test (P value=0.11), the *pad2-1* hazard ratio

is not distinguishable from the base line (hazard ratio of Col-0 inoculated line against itself=1; $\text{Log}_{10}(\text{Hazard ratio})=0$).

Figure S12. CDNB application causes a reduction in plant cellular glutathione and suppresses flg22-triggered ROS burst.

(a) Total glutathione content in *N. benthamiana* tissues after an overnight treatment with different concentrations of 1-chloro-2,4-dinitrobenzene (CDNB). Values are average \pm SE (n=3). (b) Oxidative burst was triggered by 50 nM flg22 in *N. benthamiana* tissues after an overnight treatment with different concentrations of CDNB, and measured in a luminol-based assay as relative luminescence units (RLU) over 60 minutes. Values are average \pm SE (n=24). Asterisks indicate significant differences compared to the mock control at $P < 0.001$. The experiments were repeated at least three times with similar results.

Figure S13. Model suggesting the impact of RipAY on redox activities regulated by glutathione and h-type thioredoxins.

FIGURE LEGENDS

Figure 1. RipAY-GFP suppresses immune responses in *N. benthamiana* leaves.

A. tumefaciens was used to induce the transient expression of RipAY-GFP in half of the leaf and GFP in the other half. **(a, b)** Oxidative burst triggered by 50 nM flg22 in *N. benthamiana* tissues 2.5 days post-inoculation (dpi) with *A. tumefaciens*, and measured in a luminol-based assay as relative luminescence units (RLU). Values are average \pm SE (n=24). **(c)** Quantitative RT-PCR analysis of *NbPR1* transcripts in *N. benthamiana* leaves, either untreated or treated with 1 mM SA for 12 h, 2.5 dpi with *A. tumefaciens*. Gene expression values are relative to the *NbEF1 α* housekeeping gene and are normalized to untreated *N. benthamiana* tissues. Values are average \pm SE (n=3). Asterisks indicate significant differences compared to the corresponding GFP control at $P < 0.001$. The experiments were repeated at least three times with similar results.

Figure 2. RipAY-mRFP localizes to cytoplasmic and nuclear plant cell compartments.

Two representative images from the observation of RipAY-mRFP and NLS-GFP co-transformed *N. benthamiana* leaf cells. The upper images are taken in the red channel, showing the localization of RipAY-mRFP, with a cytoplasmic and nuclear localization. The lower images, taken in the green channel, show the nuclear localization of NLS-GFP, with strong accumulation in the nucleolus. Each square has a real-life size of 164 μ m.

Figure 3. RipAY associates with h-type thioredoxins in plant cells.

GFP or RipAY-GFP were co-expressed with plant h-type thioredoxins in *N. benthamiana* before immunoprecipitation using GFP-trap beads. **(a)** RipAY association with the indicated h-type thioredoxins from *N. benthamiana* (NbTRX-h). **(b)** RipAY association with the indicated h-type thioredoxins from Arabidopsis (AtTRX-h).

Immunoblots were analysed using anti-GFP or anti-FLAG antibody. CBB, Coomassie Brilliant Blue. Molecular weight (kDa) marker bands are indicated for reference. The experiments were repeated three with similar results.

Figure 4. RipAY cysteine 333 is not critical for RipAY functions in *N. benthamiana*.

(a) Suppression of flg22- triggered ROS burst by RipAY-GFP and RipAY-C333S-GFP variant transiently expressed in *N. benthamiana* leaves. *A. tumefaciens* was used to induce the transient expression of RipAY-GFP (or RipAY-C333S-GFP) in half of the leaf and GFP in the other half. Oxidative burst was triggered by 50 nM flg22 in *N. benthamiana* tissues 2.5 days post-inoculation (dpi) with *A. tumefaciens*, and measured in a luminol-based assay as relative luminescence units (RLU). Values are average \pm SE (n=24), and are represented as percentage of the corresponding GFP control. Asterisks indicate significant differences compared to the corresponding GFP control at $P < 0.001$. **(b)** Association between RipAY-C333S or RipAY-E216Q variants and *N. benthamiana* h-type thioredoxins. GFP, RipAY-GFP, RipAY-C333S-GFP or RipAY-E216Q-GFP were co-expressed with NbTRX-h-09-FLAG and NbTRX-h-15-FLAG before immunoprecipitation using GFP-trap beads. Immunoblots were analysed using anti-GFP or anti-FLAG antibody. CBB, Coomassie Brilliant Blue. Molecular weight (kDa) marker bands are indicated for reference. The experiments were repeated three times with similar results.

Figure 5. RipAY displays GGCT activity in plant cells, which is required to degrade glutathione and suppress immune responses.

(a) Total glutathione content in *N. benthamiana* tissues 1, 2 or 3 days post-inoculation (dpi) with *A. tumefaciens* inducing the expression of GFP, RipAY-GFP or RipAY-E216Q-GFP. Values are average \pm SE (n=3). **(b)** *A. tumefaciens* was used to induce the transient expression of RipAY-GFP (or RipAY-E216Q-GFP) in half of the leaf and GFP in the other half. Oxidative burst was triggered by 50 nM flg22 in *N. benthamiana* tissues 2.5 dpi with *A. tumefaciens*, and measured in a luminol-based assay as relative luminescence units (RLU). Values are average \pm SE (n=24), and are represented as percentage of the corresponding GFP control. **(c)** Quantitative RT-PCR analysis of *NbPR1* transcripts in *N. benthamiana* leaves, either untreated or treated with 1 mM SA for 12 h, 2.5 dpi with *A. tumefaciens*. Gene expression values are relative to the *NbEF1 α* housekeeping gene and are normalized to untreated *N. benthamiana* tissues. Values are average \pm SE (n=3). Immunoblots were analysed using anti-GFP antibody to verify protein accumulation. Asterisks indicate significant differences compared to the corresponding GFP control at $P < 0.001$. The experiments were repeated three times with similar results.

TABLES

Table 1: Thioredoxin peptides identified in LC-MS/MS analysis after purification of RipAY-GFP and RipAY-HA-StrepII from *N. benthamiana* leaves.

	Gene name	Gene number	Exclusive unique peptide count	Protein Coverage (%)	Best mascot ion score
RipAY-GFP purification					
	Thioredoxin H type	NbS00049748g0003.1	5	56	120
	Thioredoxin H type 1	NbS00034448g0009.1	14	82	119
	Thioredoxin H type 1	NbS00026639g0011.1	5	81	124.8
	Thioredoxin H type 2	NbS00012766g0011.1	7	76	95.1
RipAY-HA-StrepII purification					
	Thioredoxin H type	NbS00049748g0003.1	5	51	91.2
	Thioredoxin H type 1	NbS00034448g0009.1	14	83	113
	Thioredoxin H type 1	NbS00026639g0011.1	5	82	125.5
	Thioredoxin H type 2	NbS00012766g0011.1	5	59	95.1

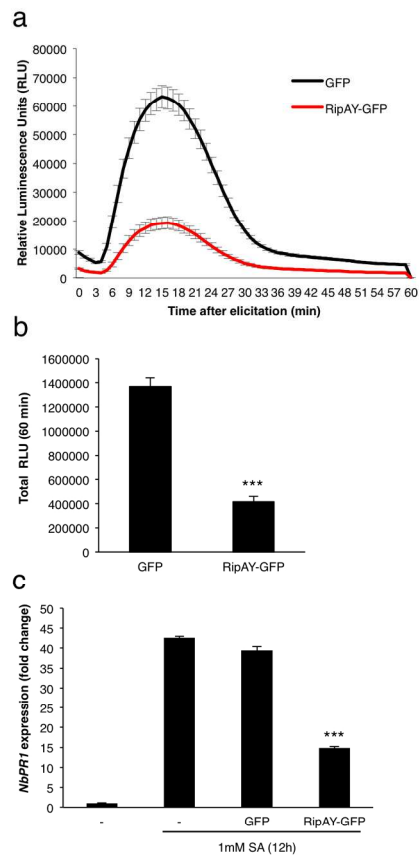


Figure 1. RipAY-GFP suppresses immune responses in *N. benthamiana* leaves.

A. tumefaciens was used to induce the transient expression of RipAY-GFP in half of the leaf and GFP in the other half. **(a, b)** Oxidative burst triggered by 50 nM flg22 in *N. benthamiana* tissues 2.5 days post-inoculation (dpi) with *A. tumefaciens*, and measured in a luminol-based assay as relative luminescence units (RLU). Values are average \pm SE (n=24). **(c)** Quantitative RT-PCR analysis of *NbPR1* transcripts in *N. benthamiana* leaves, either untreated or treated with 1 mM SA for 12 h, 2.5 dpi with *A. tumefaciens*. Gene expression values are relative to the *NbEF1a* housekeeping gene and are normalized to untreated *N. benthamiana* tissues. Values are average \pm SE (n=3). Asterisks indicate significant differences compared to the corresponding GFP control at $P < 0.001$. The experiments were repeated at least three times with similar results.

606x876mm (72 x 72 DPI)

AC

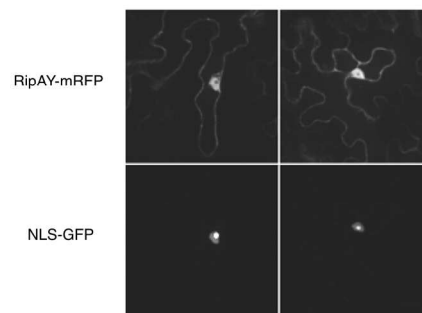


Figure 2. RipAY-mRFP localizes to cytoplasmic and nuclear plant cell compartments. Two representative images from the observation of RipAY-mRFP and NLS-GFP co-transformed *N. benthamiana* leaf cells. The upper images are taken in the red channel, showing the localization of RipAY-mRFP, with a cytoplasmic and nuclear localization. The lower images, taken in the green channel, show the nuclear localization of NLS-GFP, with strong accumulation in the nucleolus. Each square has a real-life size of 164 μm .

606x876mm (72 x 72 DPI)

AC

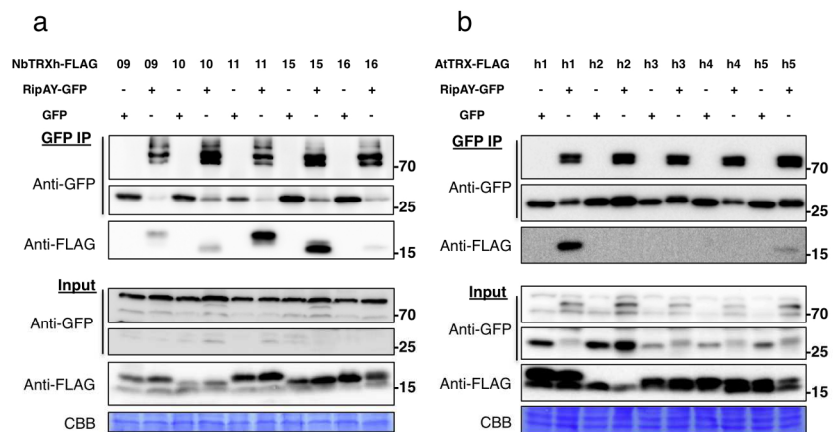


Figure 3. RipAY associates with h-type thioredoxins in plant cells.

GFP or RipAY-GFP were co-expressed with plant h-type thioredoxins in *N. benthamiana* before immunoprecipitation using GFP-trap beads. **(a)** RipAY association with the indicated h-type thioredoxins from *N. benthamiana* (NbTRXh). **(b)** RipAY association with the indicated h-type thioredoxins from *Arabidopsis* (ATR-Xh). Immunoblots were analysed using anti-GFP or anti-FLAG antibody. CBB, Coomassie Brilliant Blue. Molecular weight (kDa) marker bands are indicated for reference. The experiments were repeated three with similar results.

606x876mm (72 x 72 DPI)

AC

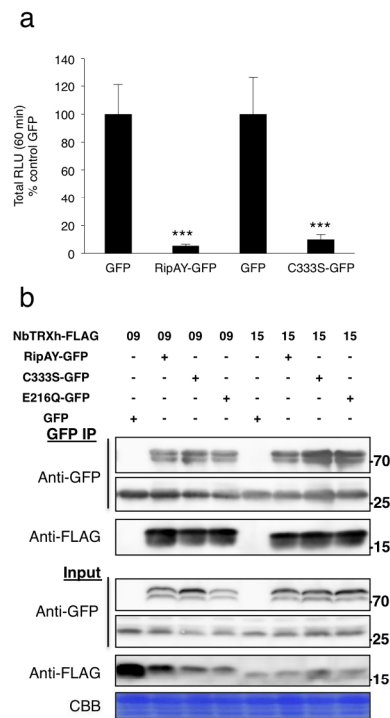


Figure 4. RipAY cysteine 333 is not critical for RipAY functions in *N. benthamiana*. (a) Suppression of flg22- triggered ROS burst by RipAY-GFP and RipAY-C333S-GFP variant transiently expressed in *N. benthamiana* leaves. *A. tumefaciens* was used to induce the transient expression of RipAY-GFP (or RipAY-C333S-GFP) in half of the leaf and GFP in the other half. Oxidative burst was triggered by 50 nM flg22 in *N. benthamiana* tissues 2.5 days post-inoculation (dpi) with *A. tumefaciens*, and measured in a luminol-based assay as relative luminescence units (RLU). Values are average \pm SE (n=24), and are represented as percentage of the corresponding GFP control. Asterisks indicate significant differences compared to the corresponding GFP control at $P < 0.001$. (b) Association between RipAY-C333S or RipAY-E216Q variants and *N. benthamiana* h-type thioredoxins. GFP, RipAY-GFP, RipAY-C333S-GFP or RipAY-E216Q-GFP were co-expressed with NbTRXh-09-FLAG and NbTRXh-15-FLAG before immunoprecipitation using GFP-trap beads. Immunoblots were analysed using anti-GFP or anti-FLAG antibody. CBB, Coomassie Brilliant Blue. Molecular weight (kDa) marker bands are indicated for reference. The experiments were repeated three times with similar results.

606x876mm (72 x 72 DPI)

AC

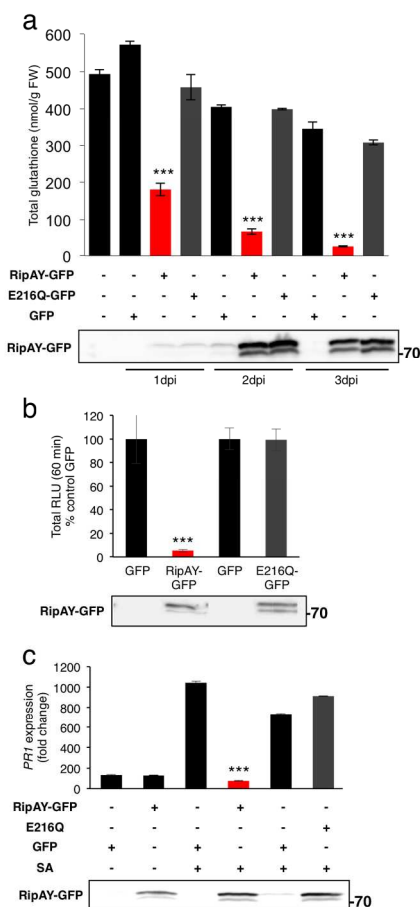


Figure 5. RipAY displays GGCT activity in plant cells, which is required to degrade glutathione and suppress immune responses.

(a) Total glutathione content in *N. benthamiana* tissues 1, 2 or 3 days post-inoculation (dpi) with *A. tumefaciens* inducing the expression of GFP, RipAY-GFP or RipAY-E216Q-GFP. Values are average \pm SE (n=3). (b) *A. tumefaciens* was used to induce the transient expression of RipAY-GFP (or RipAY-E216Q-GFP) in half of the leaf and GFP in the other half. Oxidative burst was triggered by 50 nM flg22 in *N. benthamiana* tissues 2.5 dpi with *A. tumefaciens*, and measured in a luminol-based assay as relative luminescence units (RLU). Values are average \pm SE (n=24), and are represented as percentage of the corresponding GFP control. (c) Quantitative RT-PCR analysis of *NbPR1* transcripts in *N. benthamiana* leaves, either untreated or treated with 1 mM SA for 12 h, 2.5 dpi with *A. tumefaciens*. Gene expression values are relative to the *NbEF1 α* housekeeping gene and are normalized to untreated *N. benthamiana* tissues. Values are average \pm SE (n=3). Immunoblots were analysed using anti-GFP antibody to verify protein accumulation. Asterisks indicate significant differences compared to the corresponding GFP control at $P < 0.001$. The experiments were repeated three times with similar results.

606x876mm (72 x 72 DPI)

AC